Self-assembly and dynamics of oxide nanorods on NiAl(110)

J. P. Pierce and K. F. McCarty
Sandia National Laboratories, Livermore, California 94551, USA
(Received 12 October 2004; revised manuscript received 9 December 2004; published 29 March 2005)

We observe the spontaneous formation of parallel oxide rods upon exposing a clean NiAl(110) surface to oxygen at elevated temperatures (850–1350 K). By following the self-assembly of individual nanorods in real time with low-energy electron microscopy (LEEM), we are able to investigate the processes by which the rods lengthen along their axes and thicken normal to the surface of the substrate. At a fixed temperature and O_2 pressure, the rods lengthen along their axes at a constant rate. The exponential temperature dependence of this rate yields an activation energy for growth of 1.2 ± 0.1 eV. The rod growth rates do not change as their ends pass in close proximity (<40 nm) to each other, which suggests that they do not compete for diffusing flux in order to elongate. Both LEEM and scanning tunneling microscopy (STM) studies show that the rods can grow vertically in layer-by-layer fashion. The heights of the rods are extremely bias dependent in STM images, but occur in integer multiples of approximately 2-Å-thick oxygen-cation layers. As the rods elongate from one substrate terrace to the next, we commonly see sharp changes in their rates of elongation that result from their tendency to gain (lose) atomic layers as they descend (climb) substrate steps. Diffraction analysis and dark-field imaging with LEEM indicate that the rods are crystalline, with a lattice constant that is well matched to that of the substrate along their length. We discuss the factors that lead to the formation of these highly anisotropic structures.

DOI: 10.1103/PhysRevB.71.125428 PACS number(s): 81.65.Mq, 68.37.Nq, 81.07.−b, 81.16.Dn

I. INTRODUCTION

Recent advances in nanoscience have shown us that we can awaken exotic, new behavior and functionality in materials by reducing their size to characteristic length scales over which certain physical processes occur. Learning to synthesize objects on the nanometer length scales at which effects like quantum confinement and spin-dependent transport can be exploited has been among the major challenges in this field.[1–3] Building nanostructures from metal oxides[4] may prove particularly useful since, even in their bulk forms, these complex materials can exhibit exotic behavior, including superconductivity and colossal magnetoresistance. Because of the slow speed, size limitations, and expense associated with lithographic approaches, many scientists have worked to get these materials to "self-assemble" into patterned nanostructures. Unfortunately, it is rarely possible to actually observe such self-assembly as it is happening. In most studies of nanostructure formation, the mechanisms by which the structures grow have to be inferred from still images recorded after a substrate is subjected to some process. This has made it difficult to obtain basic knowledge that would allow us to understand how self-assembly occurs and to apply it more often.

One approach to self-assembling metal oxide nanostructures on surfaces has been the oxidation of metallic alloys. In fact, the self-assembly of one-dimensional, ribbonlike nanostructures appears to be quite prevalent during the oxidation of bimetallic alloy surfaces.[5] Particularly striking examples are found in static, room-temperature STM images recorded after high-temperature oxidation of the CoGa(001) (Ref. 6) and NiAl(001) (Ref. 7) surfaces. In each case, the heat of formation of the oxide of one of the alloy's constituents (Ga and Al, respectively) is much higher than that of the other element. The resulting oxides are thought to contain only one cation species (Ga_2O_3 and Al_2O_3) and form crystalline nanorods along the [100] and [010] directions of their templates. The growth of these high-aspect-ratio structures has been proposed to result from anisotropic strain. That is, the lattice parameters of the oxide are well matched to those of the substrate along the rod axis but not along the perpendicular direction.

In this article, we show that high-temperature oxidation results in the spontaneous formation of nanorods on the (110) surface of NiAl as well. We present the results of both static and *dynamic* measurements that reveal the processes by which the nanorods assemble. In particular, by using low-energy electron microscopy[8] (LEEM) to observe their formation in real time, we are able to determine how the nanorods lengthen, grow vertically, and interact with the atomic steps of the substrate. In addition, we investigate how changes in the oxygen supply and temperature affect the growth dynamics.

NiAl is known to be useful as an oxidation-resistant material, and several groups have investigated the oxidation of its surfaces.[5,7,9–20] Early work[9] showed that many different oxide phases, including the α, δ, γ, and θ polymorphs of Al_2O_3 and the compound $NiAl_2O_4$, can form and protect the surface from further oxidation. These oxides all contain close-packed oxygen planes and are distinguished by the distribution of metal cations at octahedral and tetrahedral sites between those planes. When prepared on NiAl(110), these oxides are oriented such that their close-packed oxygen planes lie parallel to the surface. The more recent studies[7,10–20] were sparked by the discovery that protective, ultrathin alumina films that were exceptionally flat and uniform could be produced on this conducting substrate. When the (110) face of NiAl is exposed to oxygen at ~550 K, an amorphous oxide develops. Subsequent annealing to 1000–1200 K leads to crystallization of the oxide to form a 5-Å-

thick alumina film. This film consists of two oxygen-aluminum bilayers and has very recently been found to have an atomic structure closely related to the kappa phase of Al_2O_3.[10] This unique system made it possible to study a technologically important, insulating oxide (Al_2O_3) with powerful, electron-based surface probes, including electron diffraction and scanning tunneling microscopy (STM), which are typically inapplicable to studies of insulating materials. The nanorod formation that we observe is entirely different from the κ-Al_2O_3 film-forming process described above. Near the end of this article, we discuss the differences in the epitaxial relationship and formation conditions that exist between the rods and the well-studied κ-Al_2O_3 films. These differences lead us to suggest that, unlike the films, the rods are composed of a spinel-like phase related to γ-Al_2O_3 and $NiAl_2O_4$.[21]

II. SYNTHESIS AND GROWTH DYNAMICS

Our LEEM and STM experiments were conducted in separate ultra high-vacuum systems with base pressures below 1.3×10^{-10} Torr. Both systems were equipped with instrumentation for Auger spectroscopy and low-energy electron diffraction (LEED). Temperatures were monitored with W–5% Re vs W–26% Re thermocouples that were spot welded to the sides of our disk-shaped crystals. A previous wavelength-dispersive electron microprobe analysis showed that our crystals were nickel rich, with a composition near $Ni_{0.57}Al_{0.43}$.[22] Our NiAl(110) surfaces were prepared by several cycles of sputtering with 700-eV Ar ions and annealing to 1200 K. The surfaces were then held at 800–1200 K and exposed to 3–20 L (1 L = 10^{-6} Torr s) of high-purity oxygen gas. Unless otherwise noted, the LEEM images that we will present were obtained in bright field—i.e., by forming an image from the specularly reflected electron beam, at an electron energy of about 4.0 V.

Nucleation and growth of nanorods during high-temperature oxidation of the substrate are evident in the two series of LEEM images in Fig. 1. Images (a) and (d) were recorded just before the oxidation process began. The curved edges of the atomic terraces—i.e., the monatomic surface steps—of the substrate can be seen in both images. As the surface was exposed to oxygen, rodlike structures formed. All of the rods were aligned along the substrate [001] direction. With continued exposure to oxygen, the rods elongated in this direction. This growth can be easily seen by comparing image (c) to (b) and image (f) to (e) in Fig. 1. Rods eventually reached lengths in excess of 25 μm.

From Fig. 1, it is evident that rods nucleated both on terraces and at steps, but that the substrate steps provided preferred sites for nucleation. By comparing image (d) to image (e), it can be seen that an atomic step that was created where a bulk dislocation terminated at the surface [marked with an arrow in image (d)] also provided a nucleation site for a nanorod. The two series of images [(a)–(c) and (d)–(f)] show that decreasing the temperature at which the substrate was exposed to oxygen resulted in an increase in the number of rods that nucleated within the field of view. This was generally the case. Specifically, we found that reducing the exposure temperature from 1150 K to 950 K increased the nucleation density of the rods by a factor of ~100.

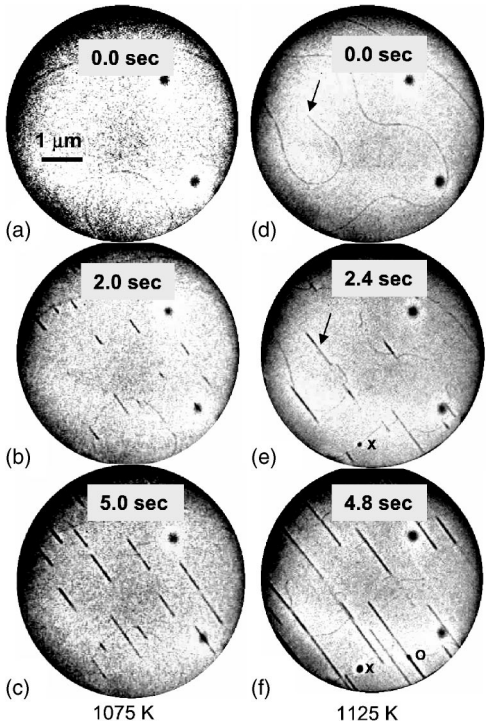

FIG. 1. Self-assembly of rod structures during high-temperature oxidation of the NiAl(110) surface. These 5-μm field-of-view LEEM images show that upon exposing the hot substrate to 1.0×10^{-7} Torr O_2, nanorods form along the substrate [001] direction. The rods elongate with continued exposure to oxygen. The two dark spots that are present in all images are a result of defective areas on our detector and are not related to the morphology of the sample.

While the nanorods grew, we often observed the nucleation of islands on the substrate that were not rod shaped. The small, dark spot to the left of the × symbol in Figs. 1(e) and 1(f) shows one such nucleation event. Diffraction analysis established that these features were patches of the well-studied κ-Al_2O_3 phase. (That is, these features exhibited the same electron diffraction pattern[11,14] as the κ-Al_2O_3 phase that is produced by low-temperature O_2 exposure followed by annealing.) This phase nucleated at substrate steps or next to the nanorods. The relative abundance of the rods and κ-Al_2O_3 on the surface could be controlled by varying the temperature at which the substrate was exposed to oxygen. After exposures at 850–950 K, κ-Al_2O_3 was virtually nonexistent. At higher temperatures and after long exposures, this phase became more abundant. This observation is consistent with those of Ref. 9, in which transmission electron microscopy (TEM) was used to analyze the oxides formed on NiAl(110) surfaces heated to 1073 K in air. In that study, transient oxide species such as spinel ($NiAl_2O_4$) and δ-Al_2O_3 formed before the more thermodynamically stable θ and γ (and presumably κ) manifestations of Al_2O_3 appeared.

LEEM gave us the unique capability to quantify the real-time growth dynamics of these structures. After nucleation, individual rods lengthened from both ends at a constant rate. In each data set in Fig. 2(a), we traced the position of one

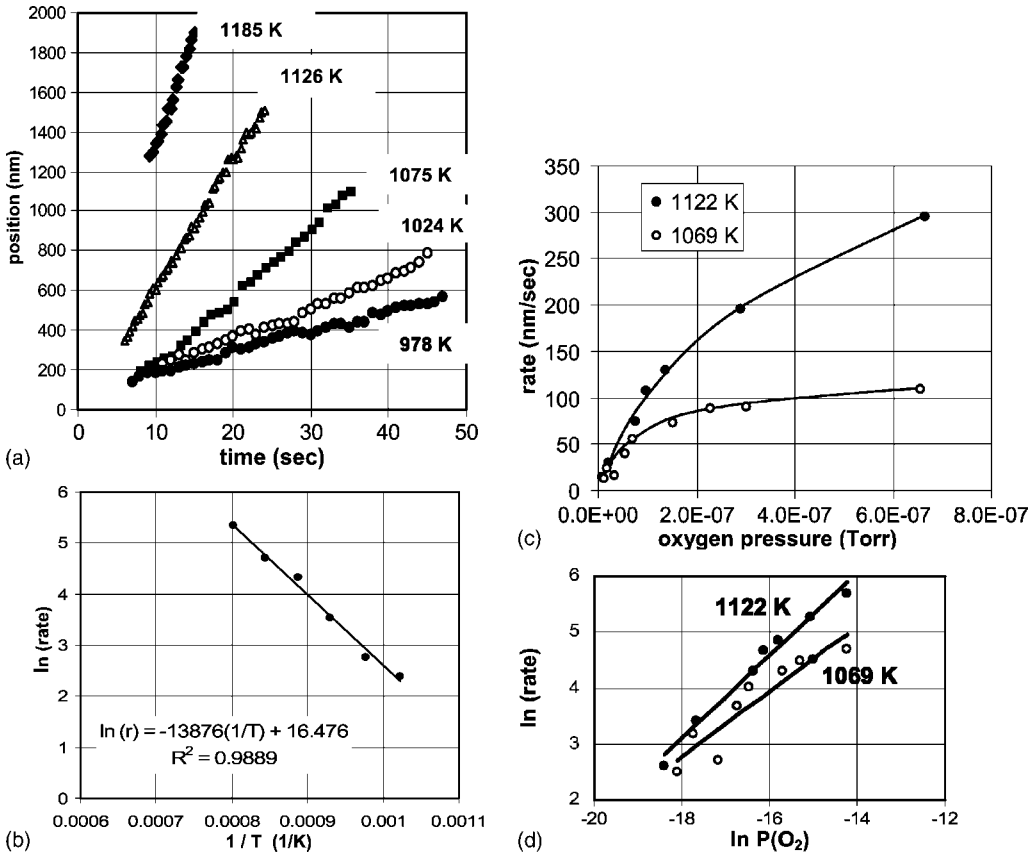

FIG. 2. Temperature and pressure dependences of the growth rate of the rod structures. (a) At a fixed oxygen pressure of 1.0×10^{-7} Torr, the ends of the nanorods were found to grow across virgin areas of the NiAl substrate at a constant rate. The data points in each curve track the position of one end of an oxide nanorod as a function of time. (b) Arrhenius plot of the temperature-dependent growth rate of the nanorods, obtained from the data in (a). The rates were measured in nm/sec. The slope is the negative of the activation energy divided by the Boltzmann constant. The plot yields an activation energy for rod growth of 1.2 ± 0.1 eV. (c) Pressure dependence of the growth rate of the rod structures. The curves that connect that data points are drawn to guide the eye. (d) A log-log plot of the data from (c). The slopes are 0.58 and 0.73 for the 1069 K and 1122 K data, respectively.

end of a given rod as a function of time during growth at five different temperatures. The constant rate of growth is evident in the linearity of the five curves. Further analysis showed that the ends of most rods within a given field of view at a given temperature elongated at the same steady rate.

At a fixed oxygen pressure of 1.0×10^{-7} Torr, the axial growth rate of the nanorods increased exponentially as the temperature was increased. The slope of the resulting Arrhenius plot [shown in Fig. 2(b)] shows that the elongation rate is limited by the kinetics of a process with an activation barrier of 1.2 ± 0.1 eV. Below, we explore the origin of this energy barrier.

In an attempt to discover the rate-limiting step in the formation of the nanorods, we investigated the effect that varying the O_2 pressure had on the axial growth rate. The results of this study are shown in Fig. 2(c). To obtain each of the curves in the figure, the substrate was held at a fixed temperature and exposed to varied O_2 background pressures. After each exposure (each data point), the sample was heated to 1350 K to sublimate the oxide before the next exposure. The data show that the growth rate does not increase linearly with the oxygen pressure. As the oxygen pressure is doubled, the axial growth rate increases by a factor less than 2, despite the fact that the local supply of oxygen has been doubled. This suggests that the arrival of metal atoms can limit the growth of the nanorods at elevated oxygen pressures.

The metal atoms could arrive at the ends of the rods via diffusion from the NiAl substrate or through the rod oxide itself. The so-called "triple defect" (two Ni vacancies and one Ni atom on an Al site) is thought to be involved in bulk mass transport in Ni-rich NiAl (Ref. 23) and could be involved in the exchange of Ni and Al atoms between the bulk and the surface during oxidation. The formation energy of this defect was measured to be 1.28 eV in Ref. 22, which is close our measured value (1.2 ± 0.1 eV) for the activation energy for nanorod growth on our Ni-rich crystal. If the metal atoms that fuel nanorod growth diffuse through the oxide itself, it would also be relevant to compare our value to activation energies for surface,[24] lattice,[25,26] and boundary[25] diffusion of cations in alumina. Unfortunately, due to difficulties described in Refs. 25 and 26, which include inconsistencies due to impurities and the long half-life of Al tracer isotopes used to measure Al diffusion, values for these energies that have been reported in the literature vary greatly and are thought to be unreliable.[25,26]

The shapes of the curves in Fig. 2(c) indicate the balance in the rates of arrival of oxygen and metal atoms at the ends of the rods. At lower pressures (say, below 2×10^{-7} Torr O_2) the growth rate is nearly linear in the oxygen pressure. In this pressure regime, the arrival of Al and/or Ni atoms is therefore nearly sufficient to accommodate an additional influx of O atoms. At higher pressures (above 2×10^{-7} Torr O_2) this is no longer true. As the number of oxygen atoms impinging on the surface is increased, it becomes more and more difficult for the influx of Al and/or Ni to keep pace with that of the O atoms. As a result, the rod growth rate is less sensitive to the oxygen pressure as the pressure is increased.

As the temperature is increased, the growth rate becomes more sensitive to the oxygen pressure. This is evident in both Figs. 2(c) and 2(d). The log-log curves in Fig. 2(d) reveal that the growth rates increase roughly as $P(O_2)^{0.58}$ and $P(O_2)^{0.73}$ at 1069 K and 1122 K, respectively. The fact that the exponent changes with temperature indicates that in this temperature-pressure regime, the growth rate is not determined by one simple process. Again, we see that the arrival rates of the two ingredients of the nanorods (oxygen atoms and metal atoms) compete in determining the growth rate. The exponent (i.e., the sensitivity of the growth rate to the oxygen pressure) is larger at 1122 K than it is at 1069 K since the diffusion of metal atoms is faster at the higher temperature and metal atoms are delivered to the ends of the rods at a higher rate. Since the metal atoms reach the ends of the rods at a higher rate, they play less of a role in limiting their growth. As a consequence, the rate at which oxygen atoms arrive (the oxygen pressure) becomes more critical in determining the growth rate and the exponent is larger than it is at the lower temperature.

It is currently unclear whether the activation barrier [see Fig. 2(b)] that limits elongation is associated with the energy barrier for the diffusion of species, either on the surface or through the bulk, or by the energy barrier for their attachment to the ends of the rods. Independent of which factor limits the growth, it is possible to estimate the area from which the ends of the rods must draw oxygen atoms in order to elongate at the observed rates. This estimate can be made by calculating the rate (R) per unit area at which oxygen atoms impinge on the NiAl surface and the rate (r) at which oxygen atoms are incorporated into the nanorods as they grow. The area is then given by the value of the ratio r/R. R can be obtained from the ion-gauge pressure during oxygen exposure (P) and the Hertz-Knudsen relation

$$\frac{R}{2} = \frac{1}{\sqrt{2\pi}}\frac{P}{\sqrt{kmT}},$$

in which k is the Boltzmann constant, m is the mass of an O_2 molecule, T is 298 K, and the factor of 2 on the left-hand side of the equation accounts for the fact that there are 2 atoms per O_2 molecule. The rate r can be estimated from the observed nanorod growth rates by assuming that the area density of oxygen atoms within a nanorod is similar to that of Al_2O_3 on NiAl(110).[27] From the data in Fig. 2(c), we estimate that rods that are 10 nm wide must draw oxygen atoms from areas 50 nm in radius surrounding the ends of the rods. In other words, all of the O atoms needed for growth can come from the O_2 that impinges on a small (50 nm radius) area around the rod ends.

If the growth rate were limited by either bulk or surface diffusion, the concentration of growth species would become depleted in a region (a "diffusion field") surrounding the active sites (the ends) of the growing rods. If two growing rods passed within each other's diffusion fields, they would compete for growth species and their growth rates would decrease. The rate at which the ends of given nanorods advanced during O_2 exposure was found to be constant, even when the ends of the rods approached within distances as low as 40 nm of each other. (This 40 nm length is the minimum separation at which we can readily resolve closely spaced nanorods in LEEM.) This observation suggests that the concentration of growth species is not noticeably depleted beyond a very small region ($<$40 nm radius) surrounding the active sites on the growing rods. In other words, if growth is diffusion limited, this observation places a rough upper bound of 40 nm on the radius of the field from which the ends of the nanorods draw atoms in order to advance. This value is consistent with the calculation above, suggesting that the atoms that are incorporated into the rods come from a small region next to their ends. These observations alone do not allow us to determine whether attachment-limited or diffusion-limited kinetics governs nanorod growth, but do allow us to conclude that if the growth rate is diffusion limited, the diffusion length is very short. Additional information in Sec. III supports the idea that diffusion, and not an attachment barrier, limits growth.

In the temperature range (850–1350 K) in which we exposed the surface to oxygen, substrate steps move significantly as the surface smooths.[22] Real-time observations showed that the steps interacted profoundly with the nanorods. A common observation was that a moving step would impinge against a rod and then flow along the rod's axis. Since the substrate steps did not flow across the rods, the rods often defined the boundary between adjacent terraces [see the STM images in Figs. 3(a) and 3(b), which will be discussed in the next section]. Another common behavior was for a step to be pinned against two parallel rods. The step segments next to the rods were connected by a curved step segment running between the rods [as in the step segment above the arrows in image 3(a)] that bulged toward the higher atomic terrace. This step arrangement results from the fact that upon cooling a NiAl crystal, atoms flow away from the surface to fill vacancies in the bulk.[22] As the surfaces in Figs. 3(a) and 3(b) were cooled from 900 K to room temperature, the upper terraces lost atoms to the bulk and the surface steps retracted in the "uphill" direction indicated by the small black arrows in the figure. The step flow was impeded where the step met the rod (i.e., the step was partially pinned). These step segments lagged behind the free segments, and the concave shape developed.

III. APPARENT HEIGHT AND VERTICAL GROWTH

Since LEEM cannot accurately measure the height and width of features as fine as the nanorods, we performed STM

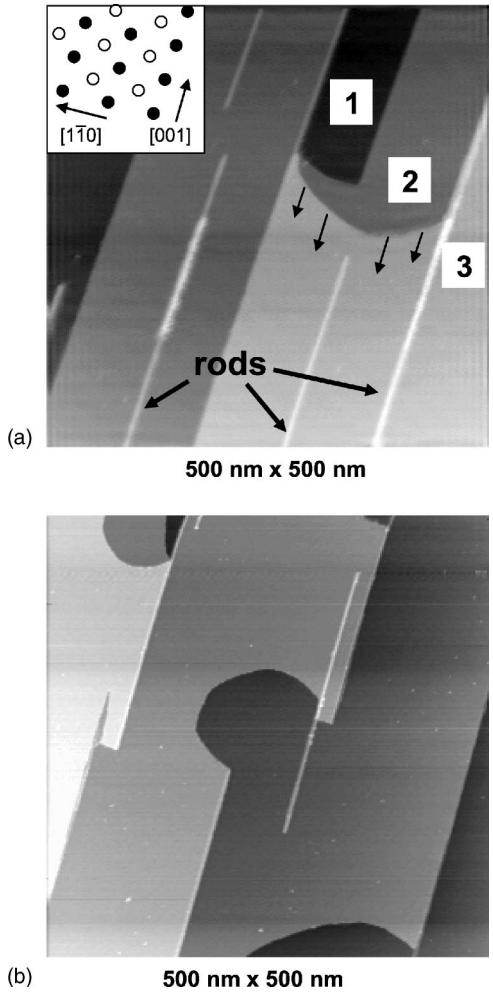

FIG. 3. Room-temperature STM morphology of the NiAl(110) surface after exposure to 1.8×10^{-7} Torr oxygen for 120 s at 900 K. Sample bias $=+3.15$ V, $I=0.19$ nA. The diagonal stripes are the oxide nanorods, which run along the substrate [001] direction. The atomic structure of the NiAl(110) substrate is shown in the inset to image (a). The lattice constants along the [001] and [1 −1 0] directions are 2.88 and 4.08 Å, respectively. Substrate terraces at three different heights (dark, medium, and light gray) are labeled 1, 2, and 3 in image (a).

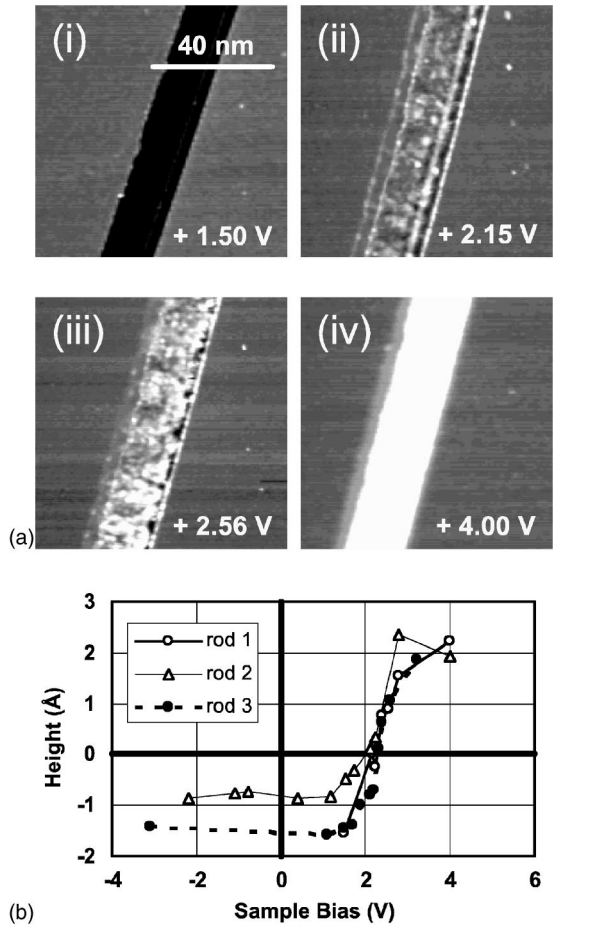

FIG. 4. Imaging bias dependence of the apparent heights of oxide nanorods in STM images. (a) Series of STM images of one nanorod recorded at different sample biases. (b) Apparent height of three representative nanorods as a function of sample bias. Rods that imaged as trenches (negative height) at low bias were always found to appear 2.0 Å high at biases greater than + 3.0 V. These rods are likely to be composed of a single oxygen-cation layer.

studies of rods grown on an identical NiAl(110) crystal to obtain more detailed information about their size and structure. Representative STM images are shown in Fig. 3. As in the LEEM images, the surfaces are marked by sharp, linear structures that run along the substrate [001] direction. As shown in the inset to Fig. 3(a), this direction is parallel to the alternating rows of nickel and aluminum atoms on the surface of the substrate. At sample biases above + 3.0 V, rods imaged as 2.0–8.0-Å-high protrusions on the NiAl surface and were between 16 and 200 Å wide. The imaging-condition-induced variations in the height of these structures will be discussed in detail below. Under particular imaging conditions, it was possible to scrape segments of the nanorods from the surface as the STM tip scanned across them. This observation suggests that the rod structures lie above the first atomic layer of the substrate and are not embedded in it. This conjecture was confirmed by contact-mode atomic force microscopy (AFM) images that were recorded in ultrahigh vacuum[28] and air after the sample was removed from the UHV chamber. The rods were observed to protrude from the surface and were structurally stable after more than 5 days of exposure to ambient conditions.

The profound dependence of the apparent height of the nanorods on the STM imaging bias is illustrated in Fig. 4. In Fig. 4(a-i), the rod images as an 18-nm-wide, 1.5-Å-deep trench at a sample bias of + 1.50 V. As the sample bias is increased [4(a-ii), 4(a-iii)], the rod images as a protrusion of increasing height. At a sample bias of + 4.0 V [Fig. 4(a-iv)], the nanorod appears as an 18-nm-wide, 2.0-Å-high protrusion. This behavior is entirely consistent with what might be expected for a wide-band-gap material on a metallic substrate. At low sample bias [+ 1.5 V in Fig. 4(a-i)], there are no available electronic states in the insulating nanorod that can contribute to the tunneling current. Instead the nanorod acts as a dielectric barrier that makes it more difficult for the electrons to tunnel from the tip to the substrate. When the tip passes over the nanorod at this relatively low bias, it must move downward in order to inject electrons into empty states

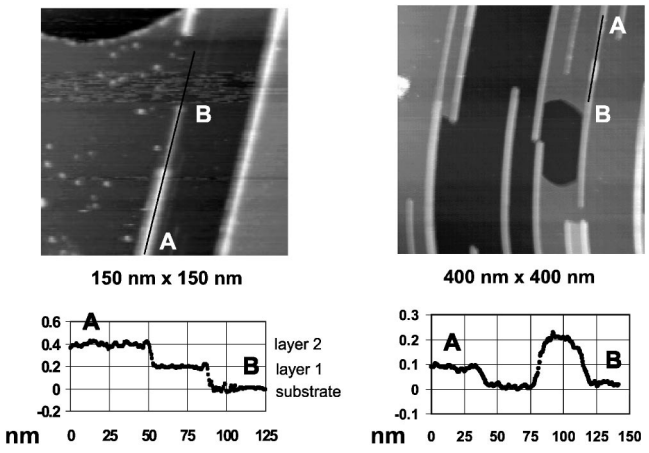

FIG. 5. Evidence for layered rod growth in STM. The STM image on the left was recorded at a sample bias of +3.15 V. Individual layers had an apparent height of 1.8–2.0 Å in images recorded at biases greater than +3.0 V. The STM image on the right was recorded at + 1.38 V. The line scan shows that this rod consists of three separate layers. Rod curvature in the right image is an instrumental artifact.

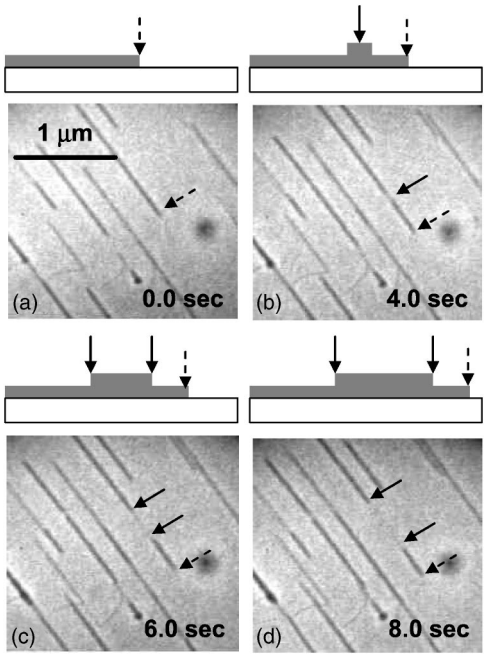

FIG. 6. Evidence for layered rod growth in LEEM. (a) The dashed arrow marks the end of a uniformly thick rod that is growing toward the lower right of the image as the substrate is exposed to 1.0×10^{-7} Torr O_2 at 1050 K. (b) The solid arrow marks the location of the nucleation of a segment of different contrast on the nanorod. Because of STM observations like those shown in Fig. 5, we attribute this change in contrast to the nucleation of a second layer. This is shown in the schematic above the image. In images (c) and (d), it is evident that the initial layer and second layer segments grow along the [001] direction with continued O_2 exposure. The areas shown are 2.3 μm wide.

of the NiAl(110) substrate and maintain the current set point. As the sample bias is raised, electrons from the tip begin to access the empty states above the band gap of the oxide nanorod. As this happens, the oxide material begins to contribute to the tunneling current and its own features begin to appear in the images. This behavior is similar to that observed during STM imaging of insulating MgO films[29] on Ag(001). In that system, the insulating MgO islands appeared as depressions until the sample bias was raised high enough to allow electrons from the tip to access empty states located above the band gap of MgO.

In studies of the bias dependence of the height of κ-Al_2O_3 films on NiAl (110), Hansen *et al.* found that the oxide's apparent height varied between 0.0 Å and 3.5 Å as the sample bias was increased from + 1.0 to + 4.2 V.[12,30] Patches of κ-Al_2O_3 had a maximum height of 3.5 Å in STM images, despite the fact that the height of this oxide phase is known to be 5.0 Å from diffraction studies.[10] Thus, STM underestimated the thickness of the oxide. With this in mind, we report the following results of our STM measurements with the understanding that the absolute heights of the oxide nanorods could differ considerably from the values that we observed. We will show that, despite this uncertainty, we can use STM to determine the number of oxygen/cation layers present in a nanorod.

A typical behavior was for rods to have an apparent height that plateaued at 2.0 Å at sample biases greater than + 3.0 V. Since the layer spacing between close-packed oxygen layers in Ni and Al oxides is typically 2.3 Å, we cautiously consider such rods to be "single-layer" rods since they are likely to be only one oxygen-cation layer in height. The curves in Fig. 4(b) are just three of several observations of this behavior in single-layer rods. At negative sample biases (i.e., in filled-state images) these rods image as trenches that are 1.0–1.5 Å deep. The apparent height remains at this level until the bias is raised to + 1.0 V, rises quickly as the sample bias approaches + 2.0 V, and finally plateaus at 1.8 to 2.0 Å at biases above + 3.0 V.[31]

The vast majority of oxide nanorods within a given imaging area are the same height. We have made several observations, however, of height changes along the length of rods that suggest that the rods can grow vertically by adding layers, as illustrated in Fig. 5. The STM image at the left of Fig. 5 shows a rod composed of segments of different heights. The line scan under the image shows that the heights of the segments are multiples of the characteristic 2.0 Å height, which, as mentioned earlier, is consistently found in images recorded at sample biases of + 3.0 V or greater. The line scan that is shown under the STM image at the right of Fig. 5 indicates that the corresponding rod is made of *three* discrete layers. The apparent layer height in that image is approximately 1 Å, which is an underestimate of the true layer height since that image was recorded with a sample bias of only + 1.35 V.

Under appropriate imaging conditions, changes in the heights of segments of the nanorods could be distinguished with LEEM as well. It was possible to monitor the individual segments both during growth and during desorption in vacuum. During growth, an additional layer often nucleated at a point on an established, single-layer rod and then grew outward toward the ends of the rod. This process is shown in Fig. 6. (We did not observe higher layers growing inward

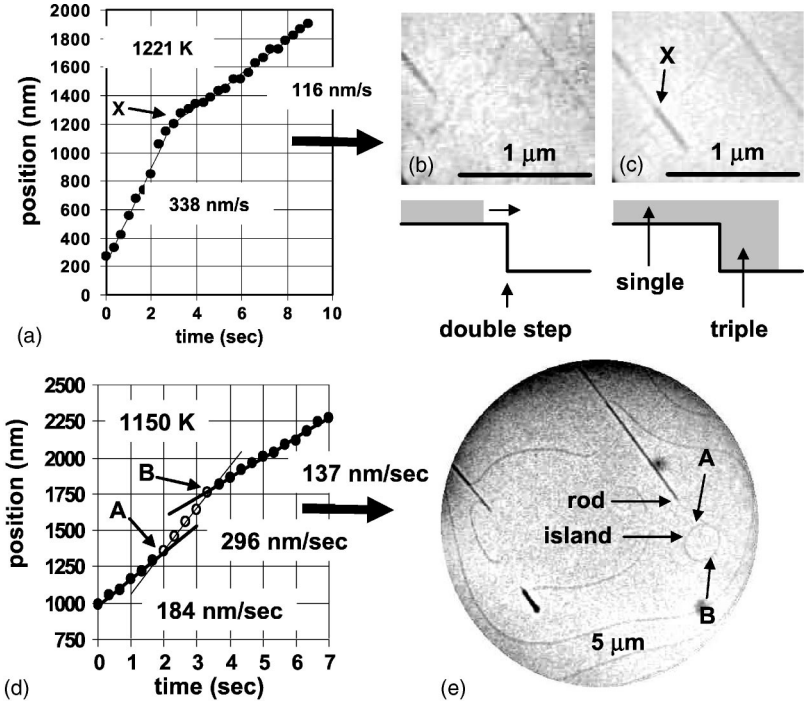

FIG. 7. Changes in rod growth rates observed as the rods cross substrate steps. In each plot in (a) and (d), the change in velocity (slope) of the nanorod growth coincides with the point in time at which the end of the rod reached the edge of a substrate terrace (point ×). The LEEM images in (b) and (c) are 1.4 μm wide and correspond to the particular rod whose growth is plotted in the curve in (a). The images were recorded before (b) and after (c) the rod crossed the substrate step (a double step) that is visible in the images. The plot in (d) and the corresponding LEEM image in (e) show a rod that gained speed as it climbed onto a monolayer-high island on the substrate (point *A*). Later, the rod lost speed as it dropped down one terrace as it reached the other side of the island (point *B*).

from the end points of the nanorods.) This layer-by-layer mode was not the only growth mode; during growth at 1000–1300 K, we often observed the appearance of multilayered rods (6–8 Å high) that proceeded as if the growth of the individual layers was simultaneous. In other words, we found that multilayer-high rods could be produced either via the addition of individual layers to existing rods or by a process in which all layers appeared at once and then grew outward, along the axis of the rod, together. Thermal desorption of the oxide nanorods could be induced by heating the crystal to 1250–1300 K in vacuum. The desorption process proceeded as the reverse of the growth process in that the rods shortened by losing material from their ends. In multilayered rods, we observed both layer-by-layer desorption and the nearly simultaneous disappearance of all layers. In both cases, the loss of material proceeded at a constant rate, and inward from the ends of the rods.

The layered nature of the nanorods profoundly impacted their growth as they elongated from one substrate terrace to the next. We often observed a sharp change in the appearance and growth rate of a rod as it encountered a substrate step. Two examples of this phenomenon are shown in Fig. 7. In each case, a sudden change in a rod's growth rate occurred precisely when the rod's end reached a step edge. Our LEEM and STM measurements have allowed us to determine the origin of this phenomenon.

In LEEM, it is straightforward to determine whether a given terrace on the NiAl surface is higher or lower than neighboring terraces by slightly changing the temperature and watching the direction of step motion. Because of mass transport between the NiAl(110) surface and the bulk of the crystal,[22] NiAl (110) islands grow (shrink) upon heating (cooling) the sample, while pits on the surface shrink (grow) upon heating (cooling). With knowledge of the local topography, we established that the rods that suddenly slowed their growth did so as they crossed from a higher terrace to a lower one. Similarly, rods that suddenly increased their rate of growth did so as they climbed up one substrate terrace.

The curve in Fig. 7(a) traces the position of the end of the rod shown in Figs. 7(b) and 7(c). Close inspection of image 7(b) reveals that the step that the rod crosses is two NiAl atomic layers high. The one-third reduction in the axial growth rate of that rod (from 338 nm/sec to 116 nm/sec) occurs exactly when the rod crosses the double step in Fig. 7(c). Given that the temperature and oxygen background pressure were held constant during growth, the supply of growth species and the probability for their attachment to the end of the rod should have also been constant. We suggest that the 1/3 reduction in the growth rate occurs because the rod shown becomes three times thicker after it crosses the step. With a fixed supply of material, growth of a rod that is 3 times as thick should be 3 times slower. With this in mind, we propose that our observations could be explained by the model shown in the schematics below Figs. 7(b) and 7(c).

Another example of this behavior can be found in the plot in Fig. 7(d), which tracks how the growth of the nanorod in Fig. 7(e) changed as it grew on and off of a single-layer-high NiAl (110) island. During the first, slower stage of growth, it is likely that the rod in Fig. 7(d) was growing as a two-layer-thick structure. When its end crossed the step (point *A*) and climbed to a higher terrace, it probably changed to a single-layer mode. If the flux of oxygen atoms and metal cations to the end of the rod was fixed, growing in single-layer mode would presumably be about twice as fast as double-layer growth. When the rod reached the other side of the island (point *B*), it dropped down one substrate terrace and began to grow in double-layer mode again. (We note that the rate of growth on the other side of the island is approximately half of the growth rate that we observed while the rod was on the island. In fact, we often observed the rates to change by

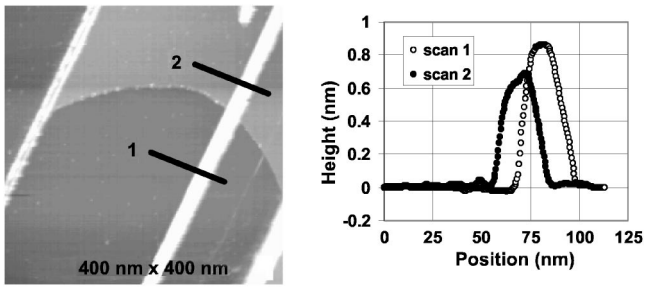

FIG. 8. STM image and linescans that show that a rod can gain or lose atomic layers upon crossing substrate steps. The relative height of the nanorod is 2 Å higher on the lower terrace (height profile 1) than it is on the upper terrace (height profile 2).

factors of approximately 1/2 or 2 at step edges.) This model is supported not only by the magnitude of the rate changes, but also by STM images such as the one shown in Fig. 8, which shows a rod that is one layer thicker on one terrace than it is on a terrace that is one atomic layer higher.

The rate changes that we observe suggest that the growth process is more likely to be governed by the barrier for diffusion of growth species to the ends of the rods rather than by the energy barrier for their attachment. To illustrate this, let us consider an event in which a nanorod climbs a substrate step. The width of the rod and the oxygen flux remain constant while the height of the nanorod decreases from two layers to one. This decrease in the rod's cross-sectional area leads to a reduction in the number of oxygen and metal atoms required to lengthen the rod. If the growth process were attachment limited, the elongation rate would be nearly independent of the rod's cross-sectional area. This is due to the fact that both the number of attachment sites and the number of oxygen atoms required to lengthen the rod scale with the cross-sectional area. In contrast, if the process were diffusion limited, the nanorod growth rate would increase (by a factor of 2 in our hypothetical example) since the fixed diffusing flux of O and metal atoms would be fueling the growth of a rod that had a smaller cross-sectional area. The diffusion-limited scenario is most consistent with our experimental findings.

IV. STRUCTURE AND COMPOSITION

Our diffraction analysis of the rods, which is summarized in Fig. 9 and its caption, provides insight into their structure. The LEEM image in Fig. 9(a) shows atomically smooth and moderately stepped regions of the NiAl(110) surface that are separated by a large step bunch that runs along the [001] direction. Because of the orientation of the step bunch, a high concentration of rods formed along it. Selected-area diffraction patterns from this region of dense rod nucleation, marked by the circle in Fig. 9(a), are shown in Figs. 9(b) and 9(d). A prominent streak of diffraction intensity runs between the NiAl diffraction spots. This streak is marked by black arrows in Fig. 9(b). The streak runs perpendicular to the rods (i.e., perpendicular to the NiAl [001] direction), as one would expect for oriented, one-dimensional structures. Indeed, dark-field microscopy shows conclusively that the

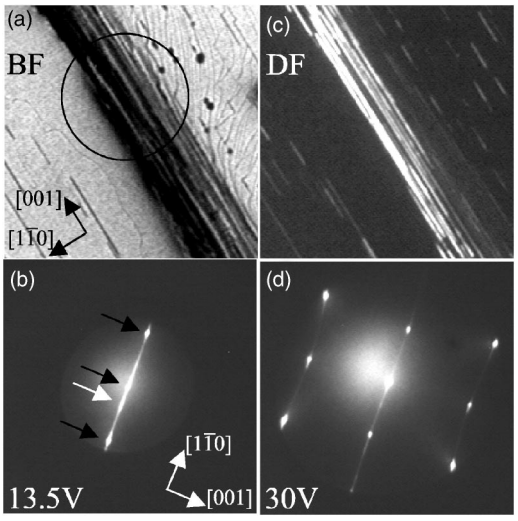

FIG. 9. Diffraction analysis of the nanorods. (a) Bright-field LEEM image of a 2.5 μm $\times$ 2.5 μm are recorded after rod growth. The dark, diagonal band is a step bunch that happens to run along the substrate [001] direction. A high concentration of rods forms along the bunch. (b) Selected-area diffraction pattern from the region within the circle of image (a). A streak of diffraction intensity runs between the diffraction spots (black arrows) of the substrate. (c) A dark-field LEEM image generated with intensity from the point on the diffraction streak indicated by the white arrow in image (b). The image shows that the rods are the origin of the streaks. (d) Higher-energy diffraction pattern showing that, with the exception of the streaks, the nanorods have no diffraction spots distinct from those of the substrate.

streaks result from the diffraction of electrons from the rods and are not diffraction intensity from either the NiAl substrate or the κ-Al_2O_3 islands. The image in Fig. 9(c) was generated with electrons that passed through a small aperture that was placed at the position along the streak shown by the white arrow in Fig. 9(b). All of the rods, including those on the step bunch and on the adjacent terraces, appear bright in this dark-field image, establishing that the rods diffract electrons into the streaks. Furthermore, the rods only appeared bright in dark-field images that were formed by selecting electrons from along the streak.

In varying the energy of the electron beam we found that, beside the diffraction streaks, the nanorods have no diffraction intensity distinct from that of the substrate. This is evident in Fig. 9(d). In particular, there was no diffraction intensity between the substrate spots along the substrate's [001] direction—i.e., along the rods. Such intensity would be expected if the lattice parameter of the rod did not match that of the substrate along its length. The streaks are oriented in the [1 −1 0] direction and are spaced by a [001] reciprocal lattice vector, suggesting crystalline order and lattice matching with the substrate in the [001] direction, with the intensity in the [1 −1 0] direction resulting from the finite width of the rods and/or atomic disorder along that direction. These streaks are completely analogous to those found in diffraction experiments on oxidized FeAl(110) surfaces.[33] This leads us to propose that self-assembled nanorods are also present in that system. Indeed, oxidation of FeAl(110) in the

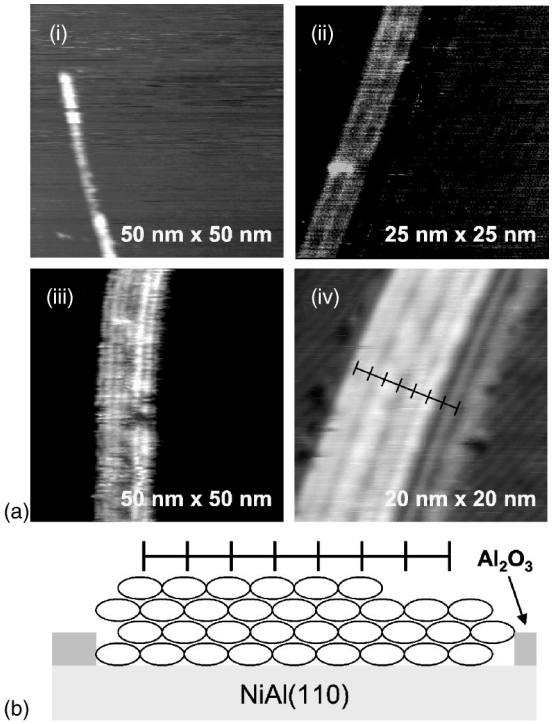

FIG. 10. (a) High-resolution STM images of oxide nanorods that reveal quantized widths. The images show that the rods are composed of parallel "subrods" that are 16 Å apart. The images show rods made of (i) one, (ii) two, (iii) seven, and (iv) six of these fundamental units. The six rods that make up the top layer of the rod in image (iv) do not completely cover the next lowest layer of the rod. (b) Schematic of the stacking of the fundamental units of the top two layers of the rod from image (a-iv).

temperature range 773–973 K produces only streaks in the LEED pattern.[33] Longer periods of oxidation at higher temperatures (~1125 K) lead to a diffraction pattern that is identical to that of a κ-Al_2O_3 film on NiAl(110).[33] It would be interesting to conduct a study like the present one on FeAl(110) substrates to confirm that nanorods can also be produced on that surface.

Analysis of high-resolution STM images reveals fundamental structure within individual nanorods. Four of these images can be seen in Fig. 10(a). Figure 10(a-iii) is a close-up of a single rod located at the edge of a NiAl(110) atomic terrace. The 2-Å height signature of the NiAl atomic step is evident in the height difference between the areas on the left and right sides of the image. The gray scale in the image has been adjusted to highlight the corrugation of the top of the nanorod. A substructure of seven rows which run along the axis of the rod is evident in the image. The rows are evenly spaced about 16 Å apart. Similar images of other rods containing one, two, and six of these 16-Å units have also been obtained and are shown in images (i), (ii), and (iv), respectively.

Figure 10(a-iv) is a 20 nm $\times$ 20 nm STM scan of an oxide rod surrounded on both sides by κ-Al_2O_3 islands. We will discuss this particular image thoroughly here, as it gives several clues as to how the growth of these nanorods proceeds. The diagonal stripe features on either side of the bold, bright rod result from the κ-Al_2O_3 unit cells (see Ref. 9), which are rotated 24° from the [001] direction. (As we discussed in Sec. II, the κ-Al_2O_3 islands are observed to grow beside the rods and not underneath them.)

The 16-Å corrugation that occurs along the width of the oxide nanorods is also visible in this particular image. Here, however, the substructure can be observed on *two* different layers. Laying an equally spaced 16-Å grid over the image shows that the height maxima of the upper layer are spatially in phase with the height minima of the lower layer. This suggests the simple model for the stacking of these fundamental units shown in the schematic in Fig. 10(b). The origin of the fundamental width units is currently unclear. One possibility is that these features correspond to the width of the unit cell of the nanorod oxide phase, just as the 9-Å- and 18-Å-spaced features that are observed in STM images of κ-Al_2O_3 are related to the large unit cell of the κ-alumina phase.[7,10,11] Another possibility is that the corrugation reflects a Moiré pattern that forms along the $[1\ -1\ 0]$ direction due to a mismatch in the lattice constants of the substrate and the oxide overlayer along that direction.

At present, the precise details of the composition and atomic registry of the rods with the substrate are unknown. The epitaxial relationship of the rods and the NiAl(110) surface provides one reason to suspect that the rods are not simply composed of the same phase of alumina (κ-Al_2O_3) that forms uniform films on this surface. As mentioned earlier, it is well known that κ-alumina prefers to grow in two domains on the NiAl(110) surface with unit cells that are rotated $\pm$ 24° with respect to the [001] direction. The rods do not form along these directions. For the structures proposed in Ref. 11 and observed in Refs. 10 and 18, the oxygen-oxygen spacing in κ-alumina on NiAl(110) is 2.98 Å. This means that a large (approximately 4.0%) lattice mismatch with NiAl would result if the close-packed oxygen rows within κ-Al_2O_3 were forced to orient along the direction in which the rods grow.

There is also evidence that the rods may not have the same elemental composition as κ-Al_2O_3. Based on the results of a TEM study by Doychak and co-workers,[9] we suggest that the rods are closely related to nickel-aluminate spinel, $NiAl_2O_4$.[21] In that study, elemental spectroscopy in the TEM showed that $NiAl_2O_4$ was the only oxide phase present during the initial oxidation of NiAl[110] at 1073 K. This is within the temperature range at which we prepared the oxide nanorods. Upon further oxidation and heating, the authors in Ref. 9 reported that the "transient" $NiAl_2O_4$ oxide slowly converted to alumina (Al_2O_3). While observing the disappearance of the nanorods during vacuum annealing in LEEM, we observed that the κ-Al_2O_3 islands grew while the nanorods shrank. That is, the rod oxide was being converted to the κ-alumina phase. It is interesting to note that the conversion process did not occur by some type of solid-state phase transformation in which the one phase was directly converted to the other. Instead, the conversion occurred as the nanorods shrunk and lost mass to the κ-Al_2O_3 islands, evidently through surface mass transport of an oxygen-containing species.

If the nanorods have a spinel-like structure,[21] determining their composition is complicated by the fact that γ-Al_2O_3

also has a spinel structure and forms a complete solid solution[9] with $NiAl_2O_4$. That is, the Ni content can vary continuously between Al_2O_3 and $NiAl_2O_4$. Clearly, the elemental composition needs to be directly measured. Some information about composition, however, might eventually be obtained via further LEEM experimentation. For example, the free energies of formation of the nanorods and the κ-Al_2O_3 islands could be determined from the equilibrium oxygen pressure of the respective phases. The formation energy of the rods would be a function of the Ni content. In addition, if the nanorods contain some Ni, their growth and abundance relative to κ-Al_2O_3 should be affected by the stoichiometry of the substrate. The calculations in Ref. 19 show that upon exposing stoichiometric or Al-rich NiAl(110) surface to oxygen, it is energetically favorable for Ni vacancies and Al anti-sites (Ni sites occupied by Al atoms) to diffuse to the surface. This process ends to depletion of Ni in the surface region and favors the formation of Al-rich oxides (κ-Al_2O_3 and $NiAl_2O_4$) at the surface. In Ref. 19, different oxidation kinetics are predicted if the substrate is Ni-rich. For Ni-rich samples, the pathways (atomic hops) that lead to Ni-depletion of the surface during O_2 exposure are 0.5 eV costlier than in Ni-depleted samples.[19] With this information in mind, we plan to investigate the high-temperature oxidation of Ni-depleted crystals. If the nanorods contain Ni, their abundance relative to κ-Al_2O_3 islands formed after given oxygen exposures should be less on a Ni-depleted crystal than on our Ni-rich substrate.

We next discuss the role of the epitaxial relationship between the nanorods and the substrate in forming these highly anisotropic structures. The TEM study by Doychak and co-workers[9] showed that $NiAl_2O_4$ was oriented such that Al_2O_3 was oriented such that its close-packed metal atoms were along the substrate [001] direction. Indeed, this is the direction along which we observed nanorod formation. The distance between neighboring metal atoms (and between neighboring oxygen atoms in the oxygen planes) in that material is approximately 2.845 Å, which is less than 1.3% smaller than the lattice constant of NiAl(110) along the [001] direction (2.882 Å). In this so-called Nishiyama-Wasserman (NW) orientation, growth of spinel along the substrate [001] direction would therefore be nearly lattice matched. The lattice matching between the cation sublattice in spinel and the aluminum atoms in the NiAl substrate is illustrated in Fig. 15 of Ref. 9. Along the substrate's [1 −1 0] direction, the respective lattice constants of NiAl and NW-oriented spinel are 4.08 Å and 4.92 Å,[9] resulting in an enormous misfit of 18.9%. In agreement with our diffraction data, this simple ball model of NW-oriented spinel on NiAl(110) predicts lattice matching with low strain along the axes of the rods and that lattice matching along the perpendicular would lead to very high strain. The resulting anisotropic strain could lead to the formation of these elongated structures. The same conclusion is reached even if the rods contain no Ni (i.e., if they consist of γ-Al_2O_3) since the lattice parameter of the γ-Al_2O_3/$NiAl_2O_4$ solid solution varies little with Ni content.[9]

While these uniaxial structures probably owe their existence to this anisotropy in the lattice matching of the oxide overlayer and the substrate, we note that a growth mechanism that does not require anisotropic lattice mismatching has been observed in TEM studies of the self-assembly of dysprosium disilicide nanowires on the Si(110) surface.[34] In those studies, high-aspect-ratio structures formed because lateral growth of the $DySi_2$ wires required a great degree of growth *into* the substrate, while lengthening of the wires did not. As mentioned earlier, our AFM studies and our ability to remove segments of the nanorods from the surface with the STM tip indicates that the nanorods lie entirely above the first atomic layer of the substrate and are not embedded in it. Confirmation by TEM that the nanorods do not grow into the substrate, however, would be desirable.

V. SUMMARY

Our combined STM and LEEM studies have allowed us to observe the self-assembly of insulating nanorods during the high-temperature oxidation of the NiAl(110) surface and have uncovered some details of the growth process. We expect that our findings related to the growth dynamics could apply to other systems, including CoGa(100),[6] NiAl(001),[7] and the (001) and (110) surfaces of FeAl.[33] On NiAl(110), rods grow along the substrate [001] direction at a constant rate that is exponentially dependent on the temperature. We find that the growth rate depends of the vertical thickness of the growing rods, but not upon their proximity to each other. The rods can grow or decompose vertically by adding or subtracting single oxygen-cation layers and come in widths that are determined by fundamental 16-Å units that form next to each other along the [1 −1 0] direction. We hope to motivate TEM studies to accurately determine the elemental makeup of the nanorods.

ACKNOWLEDGMENTS

The authors thank Dean Dibble for sharing his AFM and for lending his expertise to this project. We also thank Norm Bartelt, François Léonard, John Hamilton, and Dania Lindenberg for their insights and helpful discussions. This work was supported by the Office of Basic Energy Sciences, Division of Materials Sciences of the U.S. Department of Energy under Contract No. DE-AC04-94AL85000.

[1] S. M. Reimann and M. Manninen, Rev. Mod. Phys. **74**, 1283 (2000).

[2] F. J. Himpsel, K. N. Altmann, G. J. Mankey, J. E. Ortega, and D. Y. Petrovych, J. Magn. Magn. Mater. **200**, 456 (1999).

[3] S. D. Bader, Surf. Sci. **500**, 172 (2002).

[4] Z. R. Dai, Z. W. Pan, and Z. L. Wang, Adv. Funct. Mater. **13**, 9 (2003).

[5] R. Franchy, Surf. Sci. Rep. **38**, 195 (2000).

[6] M. Eumann, G. Schmitz, and R. Franchy, Appl. Phys. Lett. **72**, 3440 (1998).
[7] R.-P. Blum, D. Ahbehrendt, and H. Niehus, Surf. Sci. **396**, 176 (1998).
[8] E. Bauer, Rep. Prog. Phys. **57**, 895 (1994).
[9] J. Doychak, J. L. Smialek, and T. E. Mitchell, Metall. Trans. A **20**, 499 (1989).
[10] A. Stierle, F. Renner, R. Streitel, H. Dosch, W. Drube, and B. Cowie, Science **303**, 1652 (2004).
[11] R. M. Jaeger, H. Kuhlenbeck, H.-J. Freund, M. Wuttig, W. Hoffmann, R. Franchy, and H. Ibach, Surf. Sci. **259**, 235 (1991).
[12] K. Hojrup Hansen, T. Worren, E. Laegsgaard, F. Besenbacher, and I. Stensgaard, Surf. Sci. **475**, 96 (2001).
[13] C. L. Pang, H. Raza, S. A. Haycock, and G. Thornton, Phys. Rev. B **65**, 201401(R) (2002).
[14] J. Libuda, F. Winkelmann, M. Baumer, H.-J. Freund, Th. Bertrams, H. Neddermeyer, and K. Muller, Surf. Sci. **318**, 61 (1994).
[15] R.-P. Blum and H. Niehus, Appl. Phys. A: Mater. Sci. Process. **66**, S529 (1998).
[16] X. Torrelles, F. Wendler, O. Bikondoa, H. Isern, W. Moritz, and G. R. Castro, Surf. Sci. **487**, 97 (2001).
[17] J. P. Roux and H. J. Grabke, Appl. Surf. Sci. **68**, 49 (1993).
[18] G. Ceballos, Z. Song, J. I. Pascual, H.-P. Rust, H. Conrad, M. Baumer, and H.-J. Freund, Chem. Phys. Lett. **359**, 41 (2002).
[19] A. Y. Lozovoi, A. Alavi, and M. W. Finnis, Phys. Rev. Lett. **85**, 610 (2000).
[20] D. R. Jennison, C. Verdozzi, P. A. Schultz, and M. P. Sears, Phys. Rev. B **59**, R15 605 (1999).
[21] $NiAl_2O_4$ and γ-Al_2O_3 have similar "spinel" structures and can form a complete solid solution,[9] with the Ni content varying between the extremes given by the chemical formulae shown. The Ni content of the rods may vary between these extremes.
[22] K. F. McCarty, J. A. Nobel, and N. C. Bartelt, Nature (London) **412**, 622 (2001).
[23] S. Frank, S. V. Divinski, U. Sodervall, and C. Herzig, Acta Mater. **49**, 1399 (2001).
[24] W. Shin, W. S. Seo, and K. Koumoto, J. Eur. Ceram. Soc. **18**, 595 (1998).
[25] J. H. Harding, K. J. W. Atkinson, and R. W. Grimes, J. Am. Ceram. Soc. **86**, 554 (2003).
[26] A. H. Heuer and K. P. D. Lagerlof, Philos. Mag. Lett. **79**, 619 (1999).
[27] The rods are most likely composed of a phase of alumina (Al_2O_3) or spinel ($NiAl_2O_4$). The various phases of alumina ($\alpha, \kappa, \gamma, \delta$) and spinel all consist of close-packed oxygen planes that are parallel to the surface of the substrate and contain about 12.6 atoms/nm^2. To estimate the rate r, we used the measured growth rates and assumed the rods were 10 nm wide and consisted of one oxygen/cation bilayer. These physical dimensions are based on our STM observations.
[28] The heights of the rods in AFM images taken in both ultrahigh vacuum and ambient conditions ranged from 2 to 10 Å. The noise level in our ultrahigh-vacuum images was too high to allow for an accurate absolute height determination based on the height of substrate steps in the images.
[29] S. Schintke and W.-D. Schneider, J. Phys.: Condens. Matter **16**, R49 (2004).
[30] Like the authors of Ref. 12, we found that the insulating κ-Al_2O_3 patches never imaged as pits, even when the sample bias was very low. The apparent heights of the films in Ref. 12 were fixed at 0.0 Å in the voltage window from -4.8 to $+1.0$ V, as if tunneling through the vacuum and the film to the NiAl substrate were negligibly different than tunneling through only the vacuum to the substrate.
[31] We note that recent scanning tunneling spectroscopy (STS) measurements (Ref. 32) have shown that the conductance of the NiAl (110) surface increases sharply as the sample bias is raised above 2 V (i.e., that there is a sharp increase in the density of empty states or the edge of a surface "pseudogap," located 2 V above the Fermi level). The increase in conductance of the NiAl (110) surface occurs at approximately the same voltage at which we observe the increase in the apparent height of the nanorods. We suggest that the onset of the empty states of the oxide plays a far more important role than those of the substrate in determining the *relative* height of the oxide. Changes in the conductivity of the substrate alone cannot explain why the rods image as trenches at low biases and as projections at high biases.
[32] N. Nilius, T. M. Wallis, M. Persson, and W. Ho, Phys. Rev. Lett. **90**, 196103 (2003).
[33] H. Graupner, L. Hammer, K. Heinz, D. M. Zehner, Surf. Sci. **380**, 335 (1997).
[34] Zhian He, M. Stevens, D. J. Smith, and P. A. Bennett, Appl. Phys. Lett. **83**, 5292 (2003).